Spin-Triplet-Mediated Up-Conversion and Crossover Behavior in Single-Molecule Electroluminescence

Gong Chen,[1,2,*] Yang Luo,[1,*] Hongying Gao,[1] Jun Jiang,[1] Yunjie Yu,[1] Li Zhang,[1] Yang Zhang,[1] Xiaoguang Li,[3,†] Zhenyu Zhang,[1,‡] and Zhenchao Dong[1,§]

[1]*International Center for Quantum Design of Functional Materials (ICQD), Hefei National Laboratory for Physical Sciences at the Microscale, University of Science and Technology of China, Hefei, Anhui 230026, China*

[2]*School of Physics and Engineering, Zhengzhou University, Zhengzhou, Henan 450052, China*

[3]*Institute for Advanced Study, Shenzhen University, Shenzhen 518060, China*

(Received 8 December 2018; revised manuscript received 22 February 2019; published 3 May 2019)

Scanning-tunneling-microscope-induced light emission serves as a powerful approach in revealing and manipulating the optical properties of molecular species, intermolecular energy transfer, and plasmon-molecule coupling. Earlier studies have established the existence of molecular up-conversion electroluminescence in diverse situations, but the underlying microscopic mechanisms are still under active debate, dominated by intermolecular triplet-triplet annihilation and plasmonic pumping. Here we report on the experimental realization of up-conversion electroluminescence from a prototypical single phthalocyanine molecule, allowing us to unambiguously rule out mechanisms based on intermolecular coupling and also offering unprecedented opportunities to elucidate much richer characteristics unforeseen in previous studies. In particular, the bias-dependent emission intensity displays three distinct regions with different nonlinear current dependences, which can be attributed to crossover behavior caused by the interplay between inelastic electron scattering and carrier-injection processes. We also develop a microscopic description to capture the essential physics involved in up-conversion electroluminescence mediated by a proper intermediate spin-triplet state.

DOI: 10.1103/PhysRevLett.122.177401

Molecular emission is an elemental and crucial process that underpins the basis of a variety of organic optoelectronic devices. Despite decades of intensive research efforts, many fundamentally important issues remain open, in part because of limitations on the experimental probes available in this field. Scanning-tunneling-microscope-(STM-) induced molecular emission has recently been demonstrated to provide unprecedented opportunities for gaining a single-molecule understanding of a rich variety of significant optoelectronic phenomena [1]. Intriguing examples include anionic fluorescence [2], relaxationless luminescence [3,4], Fano resonance [5–7], intermolecular energy transfer [8,9], and molecular electrofluorochromism [10], all of which may play significant roles in optimizing the performance of optoelectronic devices. Up-conversion electroluminescence (UCEL), a conceptually counterintuitive phenomenon in which the emitted photon has a higher energy than that of the excitation electron, has also been observed in molecular emission from biased STM junctions [3,10–16], thereby opening new doors for the exploration of novel spectroscopic and energy devices [17].

Despite its apparent technological significance, the underlying microscopic mechanisms involved in UCEL under diverse physical situations remain perplexingly puzzling. To enable up-conversion, an intermediate state for energy relaying or a higher-order excitation process must be invoked to capture multiples of the energy quanta from the excitation source. Representative mechanisms proposed in earlier studies of UCEL within STM junctions include intermolecular triplet-triplet annihilation (TTA) [12,13] and molecular-vibration-assisted plasmonic pumping [3,18]. However, all of those observations were made on molecular multilayers, hindering potential differentiation of the competing mechanisms and identification of the dominant mechanism. It is therefore imperative to carry out control experimental studies of UCEL at the single-molecule level, which are potentially able to deliver hard data at the highest accuracy.

In this Letter, we carry out a systematic study of UCEL from a prototypical single phthalocyanine (H_2Pc) molecule in the STM tunnel junction at low tunneling currents, enabling us to gain a definitive understanding of the phenomenon in several essential aspects. First, we safely rule out the intermolecular TTA as the dominant mechanism based on the single-molecule nature of the experiment. Second, pronounced UCEL is observed even at the low-current subnanoampere level, which is at least 2 orders of magnitude lower than that typically used in plasmonic UCEL within pure metallic junctions [19–21], thereby ruling out higher-order tunneling as the dominant mechanism. Our single-molecule setup also enables us to uncover, for the first time, the existence of three distinct regions of

the emission intensity as the bias voltage increases, and each region is further characterized by its distinct nonlinear current dependence. Based on these unique experimental findings, we develop a novel microscopic spin-triplet-mediated UCEL picture that also emphasizes the delicate competition between inelastic electron-molecule scattering and carrier-injection processes, thereby resulting in cross-over behaviors in the intensity-bias relationship. These central findings may prove to be instrumental in the future design of organic optoelectronic devices with optimized performances.

In STM junctions, highly localized tunneling electrons can be used to excite a molecule electronically decoupled from the substrate. The excited molecule, in turn, can emit its characteristic light, and the radiative deexcitation rate can be greatly enhanced by the nanocavity plasmons (NCPs) [2,3,8–10,22–24], as schematically shown in Fig. 1(a) (see Sec. S1 in Ref. [25] for experimental details). A typical STM image is given in Fig. 1(b), showing five isolated H_2Pc molecules electronically decoupled by a two-monolayer- (ML-) thick NaCl spacer [22]. We stress that, given the relatively large intermolecular distance and the highly localized nature of the tunneling electrons, the measured optical properties can be ensured to be from a single molecule selected underneath the tip [8,9].

In Fig. 1(c), we show the optical spectra from a single H_2Pc molecule adsorbed on the 2ML-NaCl/Ag(100) surface at different negative bias voltages with a low current of 100 pA. The sharp emission peaks observed at

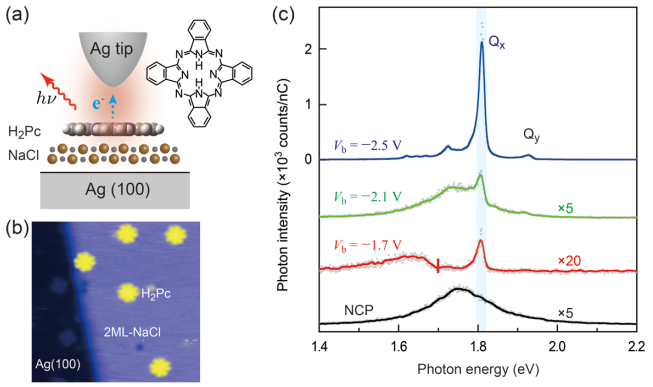

FIG. 1. Up-conversion electroluminescence from single H_2Pc molecules. (a) Schematic of the STM-induced single-molecule emission. A top view of the molecular structure is given on the right. (b) A typical STM image showing five isolated H_2Pc molecules on a 2 ML NaCl island with the characteristic eight-lobe patterns (−2.5 V, 20 pA). (c) Electroluminescence spectra from a single H_2Pc molecule at different bias voltages of $V_b = -1.7$, −2.1, and −2.5 V (100 pA, 30 s). The NCP emission spectrum from the 2ML-NaCl/Ag(100) system acquired at $V_b = -2.5$ V is also shown to reveal its broad emission feature and its potential role in resonantly enhancing the molecular optical transitions. The short vertical dash in the red curve labels the maximal energy of incident electrons.

$V_b = -2.5$ V can be assigned to the transitions from the two lowest-lying singlet states Q_x (∼1.81 eV) and Q_y (∼1.92 eV) to the ground state S_0 of the neutral H_2Pc molecule [6,9]. We call such luminescence "normal" molecular electroluminescence, since the energy of a tunneling electron (∼2.5 eV) is higher than either the optical gap of the molecule (∼1.81 eV) or the energy of the emitted photons. Of particular interest is the emission spectrum acquired at $V_b = -1.7$ V, where UCEL takes place with a clear emission peak Q_x at 1.81 eV. Furthermore, as shown in Fig. 2(a), a distinct UCEL feature can already be observed around −1.2 V, while it is absent at −1.1 V, indicating that a special excitation channel is activated at the onset voltage within the range of −1.1 to −1.2 V. Here we note that a related observation suggesting the possible existence of UCEL has also been reported in Ref. [10].

The remaining presentation is devoted to identifying the dominant microscopic mechanism for single-molecule UCEL, an effort that also leads to the observation and better understanding of richer phenomena at higher biases. Several mechanisms for UCEL prevailing in the literature can be readily ruled out for the present system. First, all the mechanisms relying on intermolecular coupling for up-conversion such as the TTA mechanism [12,13,39] can be safely excluded due to the single-molecule nature in the present experiment. Second, given the very low tunneling currents and low temperature here, mechanisms that invoke higher-order tunneling or thermally assisted processes are also very unlikely. In particular, the higher-order tunneling mechanism cannot be dominating, because otherwise the corresponding up-conversion should have taken place at the onset voltage of −0.9 V (i.e., one-half of the molecular optical gap) [21] instead of over −1.1 V shown in Fig. 2(a).

Upon excluding the prevailing mechanisms outlined above, the leading remaining UCEL mechanism is via an intermediate relay state with a significantly long lifetime. To further identify the nature of the relay state, we recall that, in this study, the typical tunneling currents are only ∼100 pA, corresponding to an average time interval of ∼1 ns between two successive tunneling electrons. Therefore, some of the widely considered states in the literatures can also be safely ruled out, such as the surface plasmon, with a typical subpicosecond lifetime [40], and the molecular vibrational modes, with a typical picosecond lifetime [41], both of which are too short to serve as relay states.

At this point, we recognize that, even though the TTA mechanism as originally proposed cannot be present in the single-molecule setup, the intrinsic spin-triplet state of the molecule may indeed serve as a relay state but within a new up-conversion framework. There are two quantitative and apparent factors that favor this potential identification: First, the UCEL onset voltage of about −1.2 V shown in Fig. 2(a) coincides with the energy of the spin-triplet

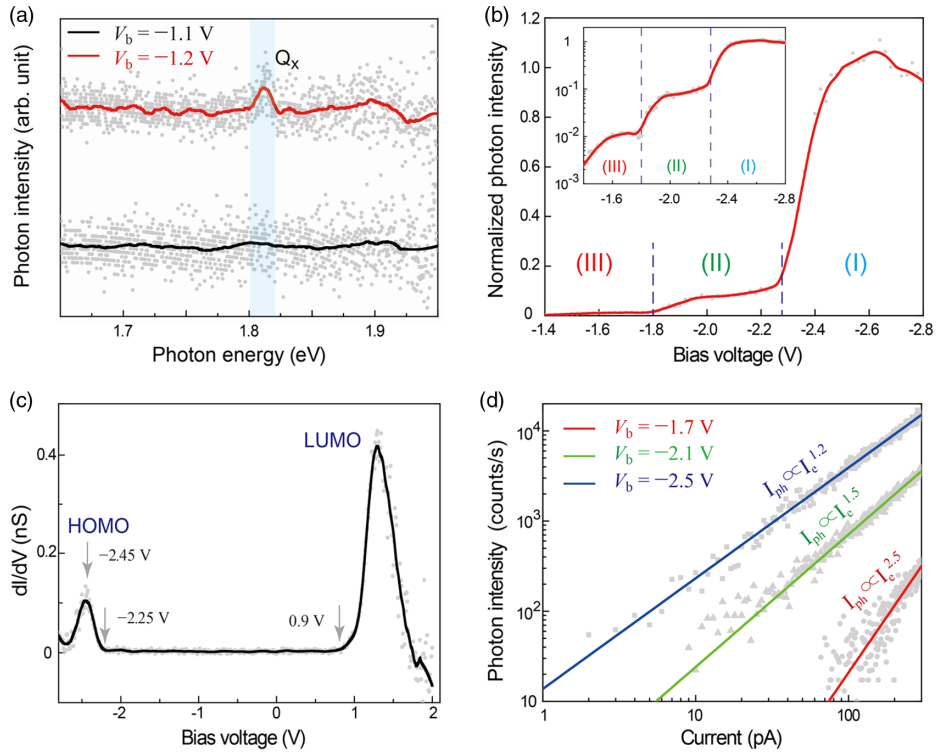

FIG. 2. Crossover behavior in single-molecule electroluminescence. (a) Electroluminescence spectra from a single H_2Pc molecule at $V_b = -1.1$ and -1.2 V (200 pA, 300 s). (b) Normalized bias-dependent intensity of the Q_x peak at a constant current of 100 pA, with the logarithmic plot shown in the inset. Here the intensity of the Q_x peak was obtained with multi-Lorentzian fitting and with the NCP background properly subtracted. (c) Differential conductance (dI/dV) of a single H_2Pc molecule, with the two peaks assigned to the HOMO and LUMO. (d) Dependence of the molecular emission intensity I_{ph} on the tunneling current I_e at three different voltages $V_b = -1.7$, -2.1, and -2.5 V.

state T_1 [42]. Second, the typical lifetime of the spin-triplet state of a free H_2Pc molecule is ~130 μs [42], much longer than the time interval between two successive tunneling electrons, enabling the state to serve as the relay state even in the physically realistic settings inside a STM junction.

Next, we develop a comprehensive picture for single-molecule electroluminescence at diverse situations that encompasses the UCEL region, with the objectives of revealing the microscopic processes involved in the excitation channels and providing compelling evidence for the importance of the T_1 state. In doing so, we have investigated the evolution of the emission intensity over a wide range of bias voltages and tunneling currents. As depicted in Fig. 2(b), the Q_x peak intensity shows three distinct stepwise increases in different voltage regions, implying the dominance of different physical processes. These three regions are defined by (I) $V_b < -2.25$ V (i.e., $|V_b| > 2.25$ V), (II) $-2.25\,\text{V} < V_b < -1.8$ V (i.e., 1.8 V $< |V_b| < 2.25$ V), and (III) -1.8 V $< V_b < -1.2$ V (i.e., 1.2 V $< |V_b| < 1.8$ V). In particular, we stress the locations of three important turning points: $V_b \approx -1.2$, -1.8, and -2.25 V, which, strikingly, coincide with the excitation energy of the spin-triplet state T_1, the optical gap between the singlet excited state S_1 and ground state S_0, and the threshold energy to extract electrons from the HOMO state of the H_2Pc molecule, respectively. The identification of the last turning point is also corroborated by the differential conductance (dI/dV) measurements shown in Fig. 2(c), where the HOMO state starts to appear at -2.25 V [43–46] (see Sec. S2 in Ref. [25]). As a side note, we also observe the existence of negative differential conductance at higher biases. The transition from region (II) to region (I) and its relation to the HOMO was previously reported in Ref. [9]. The three regions can further be distinguished by their characteristic current dependences, as shown in Fig. 2(d). Specifically, it is close to linear in region (I) but nonlinear in the other two regions; in particular, the dependence is highly nonlinear in the UCEL region (III).

To interpret the experimental observations surrounding the existence of the three electroluminescence regions, we propose a coherent microscopic theoretical framework, as depicted in Fig. 3, with some of the important model parameters obtained from first-principles calculations within density functional theory (see Sec. S3 in Ref. [25] for more details). Here we focus on the direct tunneling-electron-induced molecular excitation mechanism rather than the indirect NCP-induced molecular

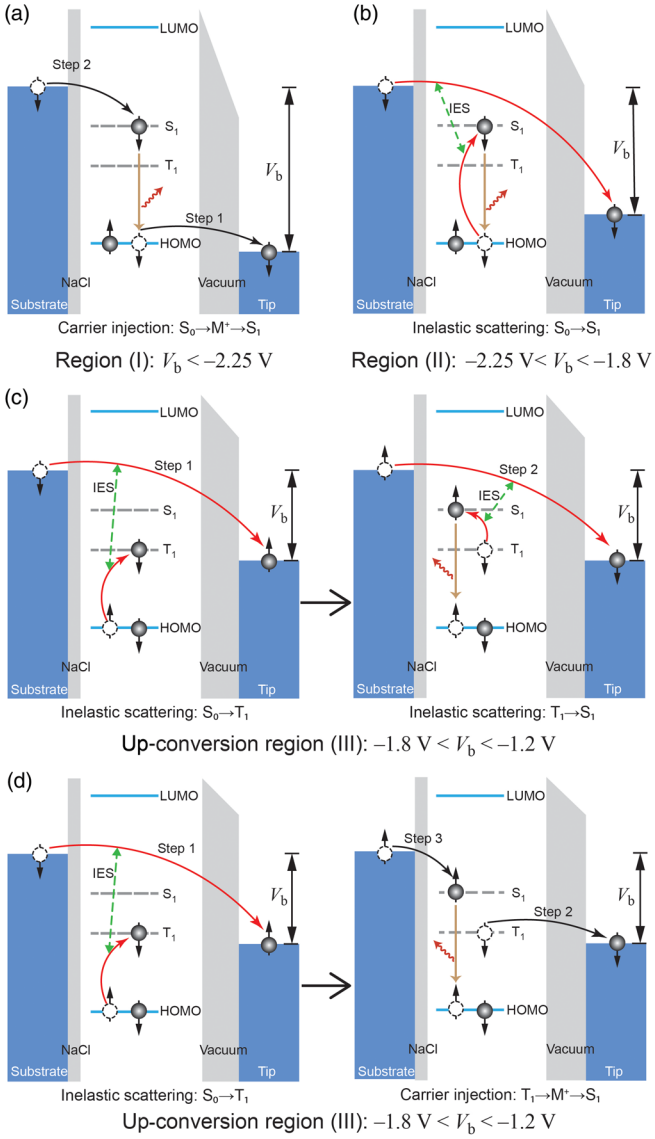

FIG. 3. Schematics on competing molecular excitation mechanisms. (a) In region (I), in which the bias window encompasses both the HOMO and S_1 states, the molecule can be excited from S_0 to S_1 by two sequential carrier-injection steps through a transient cationic state M^+ (not explicitly shown). (b) In region (II), both the HOMO and LUMO are outside the bias window, but the bias potential $|eV_b|$ is larger than the excitation energy of S_1; in this case, the molecule can be excited from S_0 to S_1 by a tunneling electron through inelastic scattering. In the up-conversion region (III), an electron can be first excited to the spin-triplet state T_1, as shown identically on the left panels in (c) and (d); subsequently, the S_1 state can be reached by either (c) an inelastic electron scattering process or (d) two sequential carrier-injection steps.

excitation mechanism [3,47–52] based on the observation of sharp molecular emission peaks; otherwise, Fano dips would be observed instead [5,6,53]. In region (I) with $V_b < -2.25$ V [Fig. 3(a)], the HOMO of the molecule lies within the bias window spanned by the Fermi levels of the tip and the 2ML-NaCl/Ag(100) substrate. In this case, the molecule can be excited from the ground state S_0 to the singlet excited state S_1 by two sequential carrier-injection (CI) steps via the transient molecular cationic state M^+ (not shown). In the first CI step, an electron in the HOMO tunnels to the tip, leaving behind a hole in the molecule. Consequently, the original LUMO of the neutral molecule becomes the LUMO of M^+, but its energy is significantly lowered due to the attractive Coulomb interaction [54,55]. Then, in the second step, another electron in the substrate can be injected into this new LUMO, which brings the molecule back to an excited neutral state S_1. Here we note that, since the electron-injection rate from the substrate to the molecule is much larger than the hole-injection rate from the tip to the molecule across the vacuum gap, the total tunneling current is limited by the hole-injection process.

In region (II) (-2.25 V $< V_b < -1.8$ V), as shown in Fig. 3(b), electron tunneling from the HOMO to the tip is energetically forbidden; therefore, the tunneling currents are dominated by the direct tunneling from the substrate through the molecule-NaCl complex to the tip. During the tunneling process, the electron can excite the molecule from the S_0 to S_1 via inelastic electron scattering (IES), which has been extensively addressed in previous studies as a valid excitation mechanism [7,10,56–65]. Given the scattering nature (i.e., with a very short electron-molecule collision time) of the excitation mechanism in region (II) relative to the carrier-injection mechanism in region (I), we naturally expect that the latter excitation channel is much more effective than the former [66]. This qualitatively explains the relative magnitudes of the emission intensities in these two regions, as experimentally observed.

In the up-conversion region (III) (-1.8 V $< V_b <$ -1.2 V), the common first step is to excite an electron into the relay spin-triplet state T_1 via the IES mechanism shown in the left panels in Figs. 3(c) and 3(d). Subsequently, there exist two possible excitation channels to further reach the S_1 state. In the first channel shown in the right panel in Fig. 3(c), a subsequent tunneling electron from the substrate to the tip can excite a metastable electron from the T_1 state to the S_1 state, again via the IES mechanism. In the second channel shown in the right panel in Fig. 3(d), the metastable electron in T_1 is able to first tunnel into the tip, enabling a subsequent electron to directly inject into the S_1 state. Here it is important to realize that, in close analogy to assessing the relative magnitudes of regions (I) and (II), the process shown in Fig. 3(d) is qualitatively stronger than that in Fig. 3(c), because the latter invokes an extra IES process. Overall, the excitation channel shown in Fig. 3(d) has to invoke either an extra IES process relative to region (I) or two extra CI steps relative to region (II); therefore, we can safely expect that the excitation efficiencies in the former two regions will be substantially higher than that in region (III). This conclusion on the relative magnitudes of the molecular emission intensities is in qualitative agreement with the experimental observations.

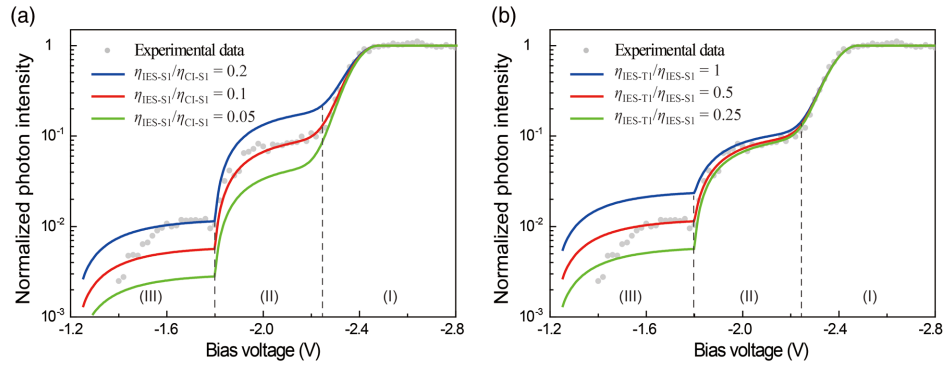

FIG. 4. Simulated crossover behavior in single-molecule electroluminescence. (a) Molecular emission intensity with different $\eta_{\mathrm{IES}-S_1}/\eta_{\mathrm{CI}-S_1}$ but at fixed $\eta_{\mathrm{IES}-T_1}/\eta_{\mathrm{IES}-S_1} = 0.25$. (b) Molecular emission intensity at optimized $\eta_{\mathrm{IES}-S_1}/\eta_{\mathrm{CI}-S_1} = 0.1$ but with different $\eta_{\mathrm{IES}-T_1}/\eta_{\mathrm{IES}-S_1}$.

The above picture can be quantitatively modeled within the framework of quantum master equations, where the populations of molecular states are determined by different excitation and deexcitation channels (see Sec. S4 in Ref. [25] for more details). Here, the observed emission intensity is proportional to the population of the S_1 state at the dynamical equilibrium. In particular, the photon intensities in the first two voltage regions are mainly determined by the excitation efficiencies of two different microscopic processes, i.e., the CI-induced S_1 excitation $\eta_{\mathrm{CI}-S_1}$ in region (I) and the IES-induced S_1 excitation $\eta_{\mathrm{IES}-S_1}$ in region (II). In contrast, in region (III), the photon intensities are determined by the multiplications of two different excitation efficiencies, namely, $\eta_{\mathrm{IES}-T_1}\eta_{\mathrm{IES}-S_1}$ in Fig. 3(c) and $\eta_{\mathrm{IES}-T_1}\eta_{\mathrm{CI}-S_1}$ in Fig. 3(d), where $\eta_{\mathrm{IES}-T_1}$ is the IES-induced T_1 excitation efficiency. Here we note that the efficiencies $\eta_{\mathrm{IES}-S_1}$ and $\eta_{\mathrm{CI}-S_1}$ in the different regions refer to the same final state but involve different initial states. The relative emission intensities between region (II) and region (I) can be approximated by the ratio $\eta_{\mathrm{IES}-S_1}/\eta_{\mathrm{CI}-S_1}$ as shown in Fig. 4(a), where we have first taken the ratio $\eta_{\mathrm{IES}-T_1}/\eta_{\mathrm{IES}-S_1}$ to be at 0.25, based on the only available quantitative transport measurements reported in Ref. [57] for pentacene molecules. Such a fitting procedure to the experimental observations yields the ratio of $\eta_{\mathrm{IES}-S_1}/\eta_{\mathrm{CI}-S_1} \approx 0.1$. Next, we tune the ratio $\eta_{\mathrm{IES}-T_1}/\eta_{\mathrm{IES}-S_1}$ as a second fitting parameter as shown in Fig. 4(b), yielding a quantitative measure of $\eta_{\mathrm{IES}-T_1}/\eta_{\mathrm{IES}-S_1} \approx 0.5$ for H_2Pc molecules. At a deeper level, in the up-conversion region, the newly identified (IES + CI)-induced S_1 excitation shown in Fig. 3(d) is ~16 times more efficient than the commonly considered (IES + IES)-induced S_1 excitation in Fig. 3(c), confirming the qualitative expectation in the last paragraph. Such quantitative information on the relative magnitudes of the microscopic processes is fundamentally important and is otherwise difficult to obtain using alternative approaches.

Before closing, we also attempt to rationalize the different current dependences in the three regions. First, given the single tunneling electron nature of the excitation channels shown in Figs. 3(a) and 3(b), a linear dependence in both regions (I) and (II) is readily expected. In contrast, for region (III), invoking two tunneling electrons, we naturally expect a quadratic current dependence. The deviations from the linear or quadratic power laws can be attributed to the emission enhancement effect associated with the stronger NCP fields as the tip-substrate gap becomes smaller [10,67]. The larger deviation from the linear power law in region (II) can be caused by an additional subtle effect; namely, when the excitation channel shown in Fig. 3(b) is activated, that shown in Fig. 3(d) is also coexisting, thereby leading to an averaged power law lying between the linear and the quadratic ones.

We have demonstrated that STM-induced luminescence serves as a powerful tool in revealing the underlying physics involved in the excitation processes of organic electroluminescence at the single-molecule level, with rich and important findings. The observation of up-conversion and crossover behavior in single-molecule electroluminescence allowed us to develop a coherent picture within the framework of quantum master equations, emphasizing the delicate competitions of the different microscopic excitation processes of inelastic electron-molecule scattering and carrier injection. Our model study not only enabled us to obtain a quantitative interpretation of the main experimental findings, but also established the vital importance of the intrinsic spin-triplet state in mediating the up-conversion electroluminescence. The insights gained in such basic studies are expected to be instrumental in the future design of novel molecular optoelectronic devices.

The authors thank Professors B. Wang, Y. Luo, and J. G. Hou for stimulating discussions. This work was partly supported by National Basic Research Program of China, National Natural Science Foundation of China, Chinese Academy of Sciences, and Anhui Initiative in Quantum Information Technologies.

*These authors contributed equally to this work.
†xgli@szu.edu.cn
‡zhangzy@ustc.edu.cn
§zcdong@ustc.edu.cn

[1] K. Kuhnke, C. Grosse, P. Merino, and K. Kern, Chem. Rev. **117**, 5174 (2017).
[2] X. H. Qiu, G. V. Nazin, and W. Ho, Science **299**, 542 (2003).
[3] Z. C. Dong *et al.*, Nat. Photonics **4**, 50 (2010).
[4] M. C. Chong, L. Sosa-Vargas, H. Bulou, A. Boeglin, F. Scheurer, F. Mathevet, and G. Schull, Nano Lett. **16**, 6480 (2016).
[5] Y. Zhang *et al.*, Nat. Commun. **8**, 15225 (2017).
[6] H. Imada, K. Miwa, M. Imai-Imada, S. Kawahara, K. Kimura, and Y. Kim, Phys. Rev. Lett. **119**, 013901 (2017).
[7] J. Kroger, B. Doppagne, F. Scheurer, and G. Schull, Nano Lett. **18**, 3407 (2018).
[8] Y. Zhang *et al.*, Nature (London) **531**, 623 (2016).
[9] H. Imada, K. Miwa, M. Imai-Imada, S. Kawahara, K. Kimura, and Y. Kim, Nature (London) **538**, 364 (2016).
[10] B. Doppagne, M. C. Chong, H. Bulou, A. Boeglin, F. Scheurer, and G. Schull, Science **361**, 251 (2018).
[11] Z. C. Dong, X. L. Guo, A. S. Trifonov, P. S. Dorozhkin, K. Miki, K. Kimura, S. Yokoyama, and S. Mashiko, Phys. Rev. Lett. **92**, 086801 (2004).
[12] T. Uemura, M. Furumoto, T. Nakano, M. Akai-Kasaya, A. Salto, M. Aono, and Y. Kuwahara, Chem. Phys. Lett. **448**, 232 (2007).
[13] T. Uemura, M. Akai-Kasaya, A. Saito, M. Aono, and Y. Kuwahara, Surf. Interface Anal. **40**, 1050 (2008).
[14] H. W. Liu, R. Nishitani, T. Z. Han, Y. Ie, Y. Aso, and H. Iwasaki, Phys. Rev. B **79**, 125415 (2009).
[15] A. Okada, K. Kanazawa, K. Hayashi, N. Okawa, T. Kurita, O. Takeuchi, and H. Shigekawa, Appl. Phys. Express **3**, 015201 (2010).
[16] A. Fujiki, Y. Miyake, Y. Oshikane, M. Akai-Kasaya, A. Saito, and Y. Kuwahara, Nanoscale Res. Lett. **6**, 347 (2011).
[17] J. Chen and J. X. Zhao, Sensors **12**, 2414 (2012).
[18] K. Miwa, M. Sakaue, and H. Kasai, Nanoscale Res. Lett. **8**, 204 (2013).
[19] G. Schull, N. Néel, P. Johansson, and R. Berndt, Phys. Rev. Lett. **102**, 057401 (2009).
[20] K. Kaasbjerg and A. Nitzan, Phys. Rev. Lett. **114**, 126803 (2015).
[21] P. J. Peters, F. Xu, K. Kaasbjerg, G. Rastelli, W. Belzig, and R. Berndt, Phys. Rev. Lett. **119**, 066803 (2017).
[22] E. Cavar, M. C. Blum, M. Pivetta, F. Patthey, M. Chergui, and W. D. Schneider, Phys. Rev. Lett. **95**, 196102 (2005).
[23] C. Chen, P. Chu, C. A. Bobisch, D. L. Mills, and W. Ho, Phys. Rev. Lett. **105**, 217402 (2010).
[24] G. Chen, X. G. Li, Z. Y. Zhang, and Z. C. Dong, Nanoscale **7**, 2442 (2015).
[25] See Supplemental Material at http://link.aps.org/supplemental/10.1103/PhysRevLett.122.177401 for experimental methods and more detailed discussion on theoretical modeling and mechanisms, which includes Refs. [26–38].
[26] P. Merino, C. Große, A. Rosławska, K. Kuhnke, and K. Kern, Nat. Commun. **6**, 8461 (2015).
[27] G. V. Nazin, S. W. Wu, and W. Ho, Proc. Natl. Acad. Sci. U.S.A. **102**, 8832 (2005).
[28] L. Edwards and M. Gouterman, J. Mol. Spectrosc. **33**, 292 (1970).
[29] S. Refaely-Abramson, R. Baer, and L. Kronik, Phys. Rev. B **84**, 075144 (2011).
[30] S. Braun, W. R. Salaneck, and M. Fahlman, Adv. Mater. **21**, 1450 (2009).
[31] S. Kubatkin, A. Danilov, M. Hjort, J. Cornil, J. L. Bredas, N. Stuhr-Hansen, P. Hedegard, and T. Bjornholm, Nature (London) **425**, 698 (2003).
[32] K. Kaasbjerg and K. Flensberg, Nano Lett. **8**, 3809 (2008).
[33] J. M. Garcia-Lastra, C. Rostgaard, A. Rubio, and K. S. Thygesen, Phys. Rev. B **80**, 245427 (2009).
[34] N. D. Lang and W. Kohn, Phys. Rev. B **7**, 3541 (1973).
[35] K. Miwa, H. Imada, S. Kawahara, and Y. Kim, Phys. Rev. B **93**, 165419 (2016).
[36] S. Prada, U. Martinez, and G. Pacchioni, Phys. Rev. B **78**, 235423 (2008).
[37] Y. Zhang, Y. Zelinskyy, and V. May, Phys. Rev. B **88**, 155426 (2013).
[38] K. Yabana and G. F. Bertsch, J. Chem. Phys. **100**, 5580 (1994).
[39] T. N. Singh-Rachford and F. N. Castellano, Coord. Chem. Rev. **254**, 2560 (2010).
[40] T. J. Y. Derrien, J. Kruger, and J. Bonse, J. Opt. **18**, 115007 (2016).
[41] V. Krishna and J. C. Tully, J. Chem. Phys. **125**, 054706 (2006).
[42] J. Mcvie, R. S. Sinclair, and T. G. Truscott, J. Chem. Soc., Faraday Trans. 2 **74**, 1870 (1978).
[43] J. Repp, G. Meyer, S. M. Stojkovic, A. Gourdon, and C. Joachim, Phys. Rev. Lett. **94**, 026803 (2005).
[44] I. Swart, L. Gross, and P. Liljeroth, Chem. Commun. **47**, 9011 (2011).
[45] S. Elke and C. J. Carlos, *Molecular Electronics: An Introduction to Theory and Experiment* (World Scientific, Singapore, 2017), Vol. 15.
[46] P. Liljeroth, J. Repp, and G. Meyer, Science **317**, 1203 (2007).
[47] G. Tian, J. C. Liu, and Y. Luo, Phys. Rev. Lett. **106**, 177401 (2011).
[48] M. C. Chong, G. Reecht, H. Bulou, A. Boeglin, F. Scheurer, F. Mathevet, and G. Schull, Phys. Rev. Lett. **116**, 036802 (2016).
[49] G. J. Tian and Y. Luo, Phys. Rev. B **84**, 205419 (2011).
[50] N. L. Schneider and R. Berndt, Phys. Rev. B **86**, 035445 (2012).
[51] S. Muhlenberend, N. L. Schneider, M. Gruyters, and R. Berndt, Appl. Phys. Lett. **101**, 203107 (2012).
[52] B. Doppagne, M. C. Chong, E. Lorchat, S. Berciaud, M. Romeo, H. Bulou, A. Boeglin, F. Scheurer, and G. Schull, Phys. Rev. Lett. **118**, 127401 (2017).
[53] H. F. Wang, G. Chen, X. G. Li, and Z. C. Dong, Chin. J. Chem. Phys. **31**, 263 (2018).
[54] J. L. Bredas, Mater. Horiz. **1**, 17 (2014).
[55] A. Rosławska, P. Merino, C. Große, C. C. Leon, O. Gunnarsson, M. Etzkorn, K. Kuhnke, and K. Kern, Nano Lett. **18**, 4001 (2018).

[56] A. Leger, M. Belin, J. Klein, and D. Defourneau, Solid State Commun. **11**, 1331 (1972).
[57] S. de Cheveigné, J. Klein, A. Léger, M. Belin, and D. Défourneau, Phys. Rev. B **15**, 750 (1977).
[58] K. W. Hipps and U. Mazur, J. Phys. Chem. **97**, 7803 (1993).
[59] E. Flaxer, O. Sneh, and O. Cheshnovsky, Science **262**, 2012 (1993).
[60] Y. Uehara and S. Ushioda, Appl. Phys. Lett. **86**, 181905 (2005).
[61] D. Ino, T. Yamada, and M. Kawai, J. Chem. Phys. **129**, 014701 (2008).
[62] P. K. Hansma, Phys. Rep. **30**, 145 (1977).
[63] R. E. Palmer and P. J. Rous, Rev. Mod. Phys. **64**, 383 (1992).
[64] H. Luth, U. Roll, and S. Ewert, Phys. Rev. B **18**, 4241 (1978).
[65] U. Roll, S. Ewert, and H. Lüth, Chem. Phys. Lett. **58**, 91 (1978).
[66] L. Sanche, J. Phys. B **23**, 1597 (1990).
[67] L. Zhang *et al.*, Nat. Commun. **8**, 580 (2017).